AIP | The Journal of Chemical Physics

A computational investigation of attrition-enhanced chiral symmetry breaking in conglomerate crystals

Francesco Ricci, Frank H. Stillinger, and Pablo G. Debenedetti

Citation: The Journal of Chemical Physics **139**, 174503 (2013); doi: 10.1063/1.4827478
View online: http://dx.doi.org/10.1063/1.4827478
View Table of Contents: http://scitation.aip.org/content/aip/journal/jcp/139/17?ver=pdfcov
Published by the AIP Publishing

A computational investigation of attrition-enhanced chiral symmetry breaking in conglomerate crystals

Francesco Ricci,[1] Frank H. Stillinger,[2] and Pablo G. Debenedetti[1,a)]
[1]*Department of Chemical and Biological Engineering, Princeton University, Princeton, New Jersey 08544, USA*
[2]*Department of Chemistry, Princeton University, Princeton, New Jersey 08544, USA*

(Received 26 August 2013; accepted 13 October 2013; published online 5 November 2013)

Attrition-enhanced chiral symmetry breaking in crystals, also known as Viedma ripening, is a remarkable phenomenon from a variety of perspectives. By providing a direct route to solid-phase homochirality in a controllable manner, it is of inherent interest to those who study chiral symmetry-breaking/amplification mechanisms. When applied to intrinsically chiral molecules, Viedma ripening may have implications for the origin of biological homochirality, as well as applications in chiral drug resolution. Despite an abundance of research, the mechanistic details underlying this phenomenon have not been unambiguously elucidated. We employ a Monte Carlo algorithm to study this driven system, in order to gain further insights into the mechanisms capable of reproducing key experimental signatures. We provide a comprehensive numerical investigation of how the model parameters (attrition rate, liquid-phase racemization kinetics, and the relative rates of growth and dissolution kinetics) impact the system's overall behavior. It is shown that size-dependent crystal solubility alone is insufficient to reproduce most of the experimental signatures of Viedma ripening, and that some form of a solid-phase chiral feedback mechanism must be invoked in order to reproduce experimentally observed behavior. In this work, such feedback mechanisms can take the form of agglomeration, or of artificial modification of the size dependent growth kinetics. © *2013 AIP Publishing LLC*. [http://dx.doi.org/10.1063/1.4827478]

I. INTRODUCTION

Attrition-enhanced deracemization[1] (also known as Viedma ripening[2]) is an intriguing phenomenon, capable of producing solid-phase homochirality. In this process, a crystalline slurry composed of a mixture of conglomerate (enantiopure) crystals is vigorously stirred in the presence of glass beads. The glass beads serve to mechanically break the crystals and maintain a large number of small crystals, thus drastically increasing the total crystal surface area. Over time, the crystalline population inexorably evolves in an acceleratory fashion to a homochiral state (e.g., 100% *S*-crystals). If the crystal population is initially composed of a racemic (∼50/50) mixture of chiral crystals, the chirality of the end state is completely random. Alternatively, if one starts with an initial chiral bias in the crystal population (i.e., a small, but measurable excess of one enantiomer over the other), the system will evolve to homochirality in the enantiomer initially in excess. Though Viedma ripening was initially demonstrated for chiral crystals composed of achiral molecules (i.e., $NaClO_3$),[1] the procedure has been extended to a wide variety of intrinsically chiral molecules that preferentially form conglomerate (enantiopure) crystals, provided that the molecules are able to interconvert at an appreciable rate via solution phase racemization. This technique has been successfully demonstrated on a range of chiral molecules, including amino acids,[3] amino acid derivatives,[4] and pharmaceutical compounds.[5] Though only ∼10% of known chiral molecules on Earth preferentially form enantiopure crystals,[6] the Viedma ripening process may have implications for the origin of biological homochirality and applications in the production of pharmaceuticals. Indeed, there have already been efforts[7] to study the scale-up of this process for pharmaceutical chiral resolution.

It is important to note that there exist certain commonalities between the various Viedma ripening experiments, which may be considered signatures of the process. Chief among these is the approximately sigmoidal evolution of the crystal enantiomeric excess ($ee^C = [N_R^C - N_S^C]/[N_R^C + N_S^C]$, where N_i^C is the number of molecules of enantiomer i in the crystal population). Experiments of Viedma ripening with crystal attrition via glass beads, and in some cases sonication, all exhibit this basic trend.[1,3–5] More recently, it has been demonstrated[2] that, for the case of explicitly chiral molecules that form conglomerates, the solution phase becomes temporarily enriched in the enantiomer which forms the minority population in the solid phase. For instance, if the crystal population evolves toward enantiopurity in the *R* enantiomer, the solution phase will become increasingly enriched in the *S* enantiomer until solid-phase homochirality is achieved, after which the solution returns to racemic equilibrium. Another interesting observation[5] was recently made during the Viedma ripening of a chemical derivative related to the blockbuster drug Clopidrogel (Plavix). After the onset of solid-phase chiral symmetry breaking, the crystal size distribution (CSD) was found to undergo a temporary widening, and

a)Author to whom correspondence should be addressed. Electronic mail: pdebene@princeton.edu

subsequently returned to its steady-state form after solid-phase homochirality was achieved.

Despite the high level of interest and the consequent accumulation of experimental findings regarding this phenomenon, there is still no general consensus regarding the key microscopic mechanisms responsible for the observations. One hypothesis[3,4] emphasizes the role of size-dependent solubility due to the Gibbs-Thompson effect,[8] and particle coarsening due to Ostwald ripening,[9] which dictates that larger crystals in a crystal population tend to grow at the expense of the dissolution of smaller crystals. According to this rationalization, an imbalance in the size distributions of left and right handed conglomerate crystals, creates a solubility-difference driving force, leading to a net higher rate of dissolution for the enantiomer with the smaller average crystal size and a net higher rate of crystal growth for the enantiomer with the larger average crystal size. As a result, if there is a difference between the crystal size distributions of the two enantiomers, the enantiomer population with the smaller average crystal size will tend to dissolve, and add to the enantiomer population with the larger average crystal size through the processes of solution-phase racemization and crystal growth. Hence, it is believed that the difference between the net rates of growth and dissolution between each enantiomer's crystal population, coupled with solution phase racemization, provide self-reinforcing effects that could drive the system inexorably to homochirality.[5]

While the continual grinding and breakage of crystals would indicate that size-dependent solubility is likely a factor in the Viedma ripening process, other hypotheses incorporate alternative microscopic phenomena as key factors underlying certain experimental signatures, such as the sigmoidal evolution of ee^C. For example, it has been postulated that small crystalline clusters, perhaps smaller than the critical size for primary nucleation, physically agglomerate on other crystals of the same handedness.[10,11] While such small crystals and/or crystalline clusters might be produced by a variety of mechanisms, we note that the chiral-symmetry breaking studies of Kondepudi[12,13] and others[14] demonstrated the formation of crystal clusters around crystals of sodium halite salts (i.e., $NaClO_3$) via "secondary nucleation." Chirality-specific agglomeration of crystals would serve as an explicit chiral feedback mechanism, effectively saving small crystals from rapidly dissolving and losing their chirality through liquid phase racemization. Recent experiments by Viedma *et al.*[15] explicitly demonstrate such chirality-specific aggregation between macroscopic crystals of sodium halite salts in a liquid-crystal slurry which is being shaken and warmed. Similar preliminary results are also shown for crystals of threonine, an explicitly chiral proteinogenic amino acid. This fascinating demonstration of macro-scale "enantiomer-specific oriented attachment" lends credence to the notion that the micro-scale agglomeration of crystals could be a factor in the Viedma ripening process, though explicit experimental validation is still needed. Aside from agglomeration, another hypothesis is that crystal-surface enhanced racemization is a key mechanism[16,17] in the Viedma ripening of chiral molecules, though this has been shown[18] to be inapplicable to several experimental systems.

Several mathematical models have been developed in an attempt to deconvolute the numerous microscopic processes which are thought to be at play. Modeling efforts have included mass-action kinetic equations,[2,10,19] classical nucleation models,[20–22] Monte Carlo (MC) simulations,[23–26] population balance approaches,[27] dispersive kinetics,[28] and agent based models.[29] All of these models are able to reproduce the sigmoidal time evolution of solid-phase enantioenrichment. Therefore, models must be able to reproduce other experimental signatures in order to test whether they can capture the essential physics of the Viedma ripening process.

Among the previous Monte Carlo studies, the work of Noorduin *et al.*[23] indicated that Ostwald ripening, attrition, and racemization are sufficient to reproduce the experimentally observed ee^C evolution. However, that model did not explicitly take into account the solution phase, and instead treated crystal growth and dissolution as the direct transfer of a molecule between crystals, with acceptance probabilities based on their relative sizes. Katsuno and Uwaha[24] developed a model that included an explicit reservoir of liquid phase molecules in contact with a crystal population. For the Katsuno-Uwaha model, Ostwald ripening, attrition, and racemization alone are insufficient; additional microscopic mechanisms must be included to reproduce the observed sigmoidal evolution of ee^C. They chose to incorporate agglomeration of small crystal clusters onto larger crystals, and in doing so were able to demonstrate the experimentally observed evolution of the crystal enantiomeric excess. While the Katsuno-Uwaha model provides an interesting Monte Carlo description of the system based on simple principles, several issues require further consideration. Mechanical attrition of crystals is manifested in this model as breakage of a crystal into two pieces of random size; however, this can only happen when a crystal grows to a predefined maximum size. As a result, the simulations evolve to an approximately uniform crystal size distribution. This is in contrast with experiments,[5] where crystal breakage may occur on crystals of varying sizes, and the CSD becomes skewed towards smaller crystal sizes, sometimes referred to as an "acceleratory" CSD.[28] The choice of parameters is such that supersaturation values in excess of 2 are reported (where the supersaturation is defined to be zero at equilibrium, as in Eq. (3) of this paper). Even allowing for the fact that this is a simple model which is not representative of true molecular scale or detail, such extreme supersaturation values are not reflective of a near-equilibrium Viedma ripening system, and serve to drastically augment the rate of crystal growth during a simulation. Crystal growth through addition/removal of individual molecules, and the agglomeration of small crystal clusters are treated with analogous phenomenological growth expressions, with the agglomeration expression containing an arbitrarily chosen supersaturation of clusters. While this choice is sufficient to reproduce the sigmoidal evolution of ee^C, no justification is provided for the rules governing agglomeration. Finally, the behavior of the solution-phase enantiomeric excess (ee^L) was not addressed, and therefore it is not clear whether the Katsuno-Uwaha model is capable of reproducing the distinctive experimental signature of temporary enantioenrichment in the minority enantiomer in the solid.

We employ a Monte Carlo algorithm to study this driven system, and to gain further insights into the mechanisms responsible for producing key experimental signatures. As pointed out by Iggland and Mazzotti,[27] modeling efforts are not only important for testing the plausibility of a proposed mechanism, but also for predicting how a system will respond to variations in process parameters (i.e., racemization rate, attrition rate, etc.). Accordingly, we perform a thorough analysis of the parameter space, and demonstrate the effects of racemization rate, attrition rate/intensity, growth/dissolution rate constants, and system size. The paper is structured as follows. In Sec. II, we describe the model and the corresponding Monte Carlo algorithm. In Sec. III, results are presented and compared to experiments. Finally, in Sec. IV concluding remarks are provided along with a discussion of ideas for future research.

II. MODEL AND NUMERICAL METHODS

To model the Viedma ripening process, we consider a distribution of conglomerate crystals, each containing "m" intrinsically chiral molecules. The crystal population is in contact with solution-phase chiral molecules, for all of which $m = 1$. This model assumes a well mixed system, which is a good approximation due to the high rate of stirring applied during experiments, and therefore we neglect spatial degrees of freedom. We also assume that the system is isothermal. Since Viedma ripening is a near-equilibrium process, we do not consider primary nucleation events, hence solution-phase chiral monomers ($m = 1$) cannot aggregate to form crystalline species. In our model, we define a crystal to be of size $m \geq 2$. As with previous modeling efforts,[23,24] we are modeling pseudo-crystals, composed of a computationally tractable number of molecular constituents.

A randomly selected chiral molecule in the solution phase attempts racemization with the following probability per unit time:

$$p_r = \exp\left(-\beta E_r\right), \tag{1}$$

where $\beta = 1/k_B T$, k_B = Boltzmann's constant, T = absolute temperature, and E_r is the activation energy for racemization. The choice of unity for the pre-exponential factor is equivalent to a choice of time unit.

A randomly selected crystal composed of m chiral molecules may either attempt to grow or dissolve by addition/removal of single molecules according to the following thermodynamically consistent phenomenological rate expression, which assumes approximately spherical crystals for simplicity:

$$j = \alpha \sigma_i m^{2/3} - \delta m^{1/3}, \tag{2}$$

where $j = \langle d/dt \rangle m$ = net rate of growth for the crystal, α = growth rate constant, σ_i = supersaturation of enantiomer i, where i is the enantiomer of the crystal in question (R or S), and δ = dissolution rate constant. The supersaturation of enantiomer i is

$$\sigma_i = \left(N_i^L - N^{eq}\right)/N^{eq}, \tag{3}$$

where N_i^L = solution-phase molecule number (concentration) of enantiomer i, N^{eq} = equilibrium solution-phase molecule number (solubility) of enantiomer i. The subscript is omitted for N^{eq} since the solubility is equal for both enantiomers $\{R, S\}$ in accordance with the Meyerhoffer double solubility rule.[30] Equation (2) is of the same form suggested by Katsuno and Uwaha,[24] and its derivation can be found in Appendix A.

In order to test the robustness of the symmetry-breaking phenomenon, we also performed simulations with a slightly modified phenomenological rate expression which assumes that the rate of dissolution is proportional to the crystal's surface-to-volume ratio, yielding a dissolution term which goes as $m^{-1/3}$. Even with this modified phenomenology, we found that the results were qualitatively identical to those presented below, which utilize Eq. (2). Selected results obtained with the modified rate expression are given in the supplementary material.[31]

The magnitude of the rate constants, α and δ, and the instantaneous value of the supersaturation, σ_i, determine the critical crystal size, m_i^*, such that crystals larger than m_i^* tend to grow and crystals smaller than m_i^* tend to shrink. By setting net crystal growth rate, j, in Eq. (2) equal to zero, we calculate the critical size as

$$m_i^* = \left(\frac{K}{\sigma_i}\right)^3, \tag{4}$$

where we have defined the ratio of rate constants, $K = \delta/\alpha$. In the event that the supersaturation is negative, the critical size is automatically set to infinity in our model. For our Monte Carlo algorithm, the probability of growth per unit time by addition of a single molecule for a crystal of size m, and handedness i is given by

$$p_g = \frac{m^{1/3}}{m^{1/3} + (m_i^*)^{1/3}}. \tag{5}$$

This expression is simply the ratio of the rate of growth to the sum of the rates of growth and dissolution. The probability of dissolution per unit time by the removal of a single molecule is taken as the complement: $p_d = 1 - p_g = (m_i^*)^{1/3}/(m^{1/3} + (m_i^*)^{1/3})$. With these probabilities, it is clear that a larger crystal has a higher probability of growth than a smaller crystal, while the latter has a higher probability of dissolution.

A randomly selected crystal can also suffer attrition. We define a minimum size for attrition, $m_{min} = 4$, at or above which a crystal may undergo attrition and below which we assume a crystal is no longer subject to breakage. The attrition rate, which is related to the amount of mechanical energy input to the system per unit time, is described by the probability per unit time that a selected crystal will successfully undergo an attrition event, p_{attr}. If successfully selected for attrition, the crystal is broken into two crystals of random size ≥ 2.

We also incorporate agglomeration into the model. Agglomeration is a complex phenomenon that occurs when crystals attach to, and can become fully incorporated into, other crystals. The basic mechanism of agglomeration[32] consists of two independent steps: the collision of two crystals (higher order collisions are neglected here for simplicity), and the

physical "sticking" of the two crystals. Hence, in the simplest model of such a process, one can express the microscopic probability of agglomeration per unit time as a combination of these two independent processes

$$p_{agglom} = p_1 p_2, \tag{6}$$

where p_1 = probability per unit time of collision between two crystals, and p_2 = probability per unit time of the contacted crystals sticking together. Following crystallization modeling efforts,[32] we developed approximations for p_1 and p_2. While the probability of two crystals of certain sizes colliding, p_1, is simply proportional to the product of their respective concentrations, the probability of the two crystals then sticking together is more complex. Previous crystallization modeling considers the formation of a crystalline bridge between the two crystals which have come into contact.[32] The building up of this bridge requires the two crystals to stay in contact long enough to crystallize the mass of the bridge from dissolved molecules in the solution, and hence it is directly dependent on the rate at which molecules are deposited onto crystals from solution. The net mass flux of molecules from solution onto the crystal surfaces is proportional to the net growth rate of the crystal population.[32] Hence, the higher the crystal growth rate, the more rapidly molecules will be deposited onto crystal surfaces, and the more rapidly crystalline bridges can be formed between crystals in contact. The recent work of Viedma *et al.*[15] clearly demonstrates the formation of such crystalline bridges between macro-scale crystals undergoing enantiomer-specific oriented attachment. Using these physical arguments, we assume the validity of the following relationships for agglomeration between crystals of the same chirality i, with sizes $m = p$ and $m = q$, respectively:

$$p_1 \sim C_p C_q, \tag{7}$$

$$p_2 \sim J, \tag{8}$$

where C_p = concentration of crystals of size p and chirality i, C_q = concentration of crystals of size q and chirality i, and J = net crystal growth rate of the overall population.

We use these assumptions to implement agglomeration in our model by allowing only the smallest crystals ($m = 2$) to agglomerate with other crystals of size $m \geq 2$. This choice is made strictly for simplicity, as done previously,[24] since the hypothesized agglomeration in Viedma ripening experiments is purportedly due to small "sub-critical clusters." Combining Eqs. (6)–(8), a randomly selected crystal of size m and handedness i may attempt an irreversible agglomeration event with the probability per unit time

$$p_{agglom} = x_i^{(2)} p_g, \tag{9}$$

where $x_i^{(2)}$ = fraction of crystals which are dimers of handedness i, and $p_g = m^{1/3}/(m^{1/3} + (m_i^*)^{1/3})$ = probability per unit time of growth of the crystal selected for agglomeration. The crystal fraction, $x_i^{(2)}$ (representing p_1 in Eq. (7)) is proportional to the concentration of dimers of handedness i, and hence proportional to the probability per unit time that the selected crystal will collide with a dimer. The probability of growth of the selected crystal, p_g (representing p_2 in Eq. (8)) determines the rate of crystal growth. This choice of p_2 implicitly introduces a size dependence to the sticking probability.[27,33] If a crystal is chosen and successfully attempts agglomeration, a dimer of the same handedness is randomly selected and added to the crystal.

Our modeling of the agglomeration process is different from that of Katsuno and Uwaha,[24] who consider this process as reversible, completely analogous with single molecule growth/dissolution, and utilize an arbitrary supersaturation of dimers as the thermodynamic driving force. Our approach to modeling agglomeration is not intended to serve as a detailed molecular description of this process. Rather, we adopt an approximate representation of a complex phenomenon, based on principles of crystal agglomeration,[32] in order to explore its effect on chiral symmetry-breaking.

With the aforementioned processes, our simple model includes the physical and chemical processes of solution-phase racemization of chiral molecules, the Gibbs-Thompson effect (size-dependent solubility, as manifested in Eq. (2)), mechanical breakage of crystals by grinding, and agglomeration. We first employ the model without agglomeration in order to see if the Gibbs-Thompson effect alone is sufficient. Since this is the most basic form of our model, we refer to it as the "elementary model." The Monte Carlo algorithm for the elementary model is as follows:

1. Initialize the simulation with a starting crystal size distribution for each enantiomer and the initial concentration of chiral molecules in the solution-phase reservoir.
2. A molecule is chosen at random.
3. If it is in the liquid phase, racemization is attempted with probability p_r. If it is in the crystal phase, a crystal of the same handedness is selected at random (irrespective of its size) with either growth, dissolution, or attrition randomly selected with equal probability, and the chosen process is attempted with its respective probability.
4. Time and system variables are updated.
5. Return to step 2, thus repeating the cycle until the specified end time.

If we wish to incorporate agglomeration, the algorithm is only slightly altered. In step 3, if a crystal-phase molecule has been randomly selected, a crystal of the same handedness is randomly selected irrespective of its size. As before, this is to ensure that all crystals are accessed with equal probability. Then either growth, dissolution, attrition, or agglomeration is randomly selected with equal probability, and the chosen process is attempted with its respective probability. Flow charts of both versions of the algorithm are included in Appendix C.

All simulations begin with a Gaussian CSD. If an initial enantiomeric excess is present in the solid, we implement it by maintaining the same mean, but decreasing the total number of crystals of one enantiomer. A typical starting CSD with a 5.5% enantiomeric excess in the crystal phase is shown in Figure 1. Once again, we define the enantiomeric excess of each phase as follows:

$$ee^{\psi} = \frac{N_R^{\psi} - N_S^{\psi}}{N_R^{\psi} + N_S^{\psi}}, \tag{10}$$

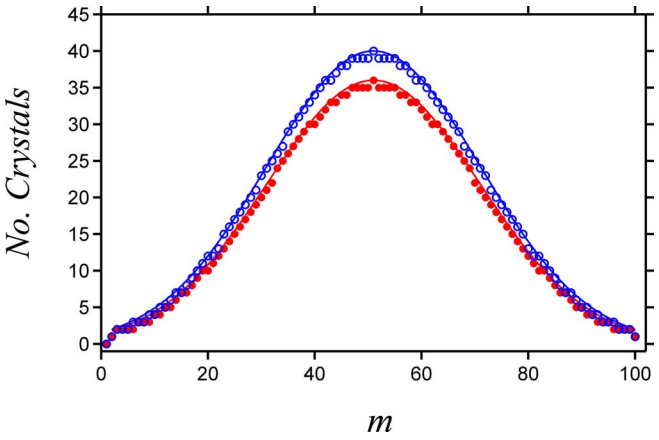

FIG. 1. Typical initial Gaussian CSD, with $ee^C(0) = 0.055$, $N_R{}^C + N_S{}^C = 186\,660$. The blue points represent the *R*-enantiomer, and the red points represent the *S*-enantiomer. The curves are the Gaussian functions from which the CSD was created, and the noise in the distribution arises from discretization. For this CSD, we define, $N^{eq} = 10\,000$, hence the simulations using this initial CSD have $N_{total} = 206\,660$.

where ψ represents the phase (crystal = *C*, solution = *L*), and N_i^{ψ} is the total number of molecules of handedness *i* in phase ψ.

Since this is a near equilibrium process, we choose to begin all simulations with the equilibrium (solubility) number of chiral molecules in the solution phase. Hence, at t = 0 we have $N_R^L(0) = N_S^L(0) = N^{eq}$. The value of N^{eq} is set based on the initial number of crystal-phase molecules. For the purposes of an efficient simulation with adequate mass-transfer between the crystal and solution phases, N^{eq} for each enantiomer is taken to be roughly one order of magnitude smaller than the total number of molecules initially in the solid, $N_R^C(0) + N_S^C(0)$. For example, for the initial CSD in Figure 1, $N_R^C(0) + N_S^C(0) = 186\,660$, and $N^{eq} = 10\,000$. For more information on variable definitions, refer to the supplementary material.[31]

III. RESULTS AND DISCUSSION

Our first aim was to determine whether our model is capable of reproducing the experimental signatures with only racemization, size dependent growth/dissolution (Gibbs-Thompson), and mechanical attrition. As previously mentioned, we refer to this as the "elementary model." A comprehensive set of simulations was performed over a large range of parameter space with the elementary model, and none of the simulations performed showed a clear resemblance to the aforementioned experimental signatures. This is illustrated in Figure 2, where the time evolution of ee^C for 100 independent simulation runs is shown. Note that a MC step is here defined as one trial event, whether successful or not.

In these simulations, the crystal phase is initially biased with $ee^C = 0.055$, which is similar to the initial bias employed in many experiments,[1,3,4] and we would therefore expect the system to evolve to enantiopurity in the direction imposed by the initial bias. In reality, however, the system evolves in an unpredictable fashion to either state of enantiopurity, while not exhibiting the experimentally observed sigmoidal evolution of the crystal enantiomeric excess. This result, which is in agreement with previous modeling efforts,[24,34] illustrates the fact that size-dependent solubility by itself is insufficient to explain Viedma ripening in our model.

The above observation suggests that, in order to reproduce the sigmoidal and bias-sensitive behaviors seen experimentally, we need to introduce a chiral feedback mechanism. This could be achieved by introducing additional mechanisms such as agglomeration, but it can also be inserted by simply modifying the phenomenological crystal growth rate expression. For the purposes of illustration, we modify Eq. (2) as follows:

$$j = \alpha\sigma_i X_i^C m^{2/3} - \delta m^{1/3}, \tag{11}$$

where X_i^C = fraction of crystals which are of handedness *i*. Inserting X_i^C introduces a chiral feedback, whereby whichever enantiomer is prevalent in the crystal phase ($X_i^C > 0.5$) gains an advantage in the growth rate over crystals of the

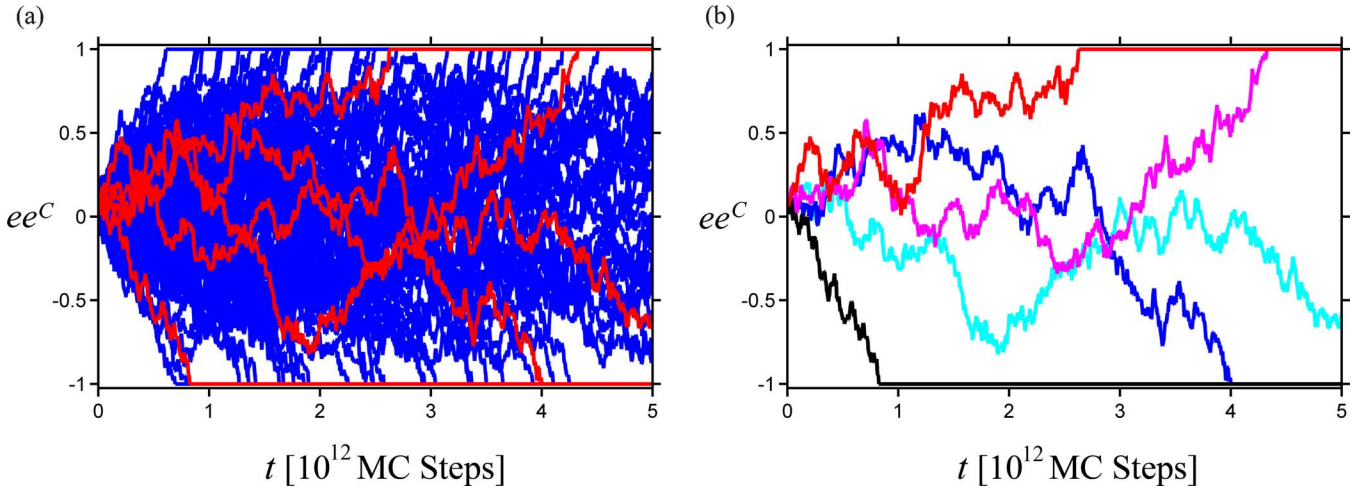

FIG. 2. Crystal enantiomeric excess trajectories for the elementary model. Simulations began with initial bias, $ee^C(0) = 0.055$. (a) 100 independent simulations, with 95 trajectories in blue and five highlighted in red for contrast. (b) The five highlighted trajectories in (a) are re-plotted, each in a different color to clearly illustrate the erratic behavior of each trajectory. All runs performed with $\beta E_r = 5$, $p_{attr} = 0.4$, $K = 1$, $N_{total} = 206\,660$, $N^{eq} = 10\,000$.

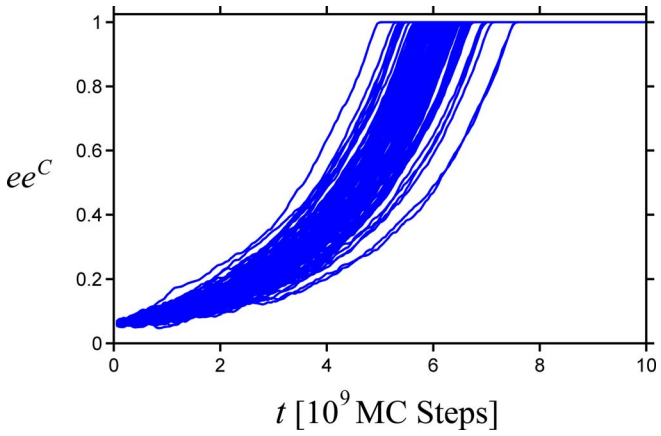

FIG. 3. Evolution of crystal-phase enantiomeric excess for the model with agglomeration. Simulations began with initial bias, $ee^C(0) = 0.055$. Trajectories of 100 independent simulation runs are shown. All simulation parameters identical to Figure 2.

opposite handedness. Solving for the critical size, we now have $m_i^* = (K/(\sigma_i X_i^C))^3$.

In the context of the current model, this nonlinearity is artificial, as the growth rate of a single crystal should not be directly influenced by the overall composition of the crystal population. However, when we insert this nonlinearity the behavior is markedly different, and our model qualitatively reproduces key experimental signatures. This is shown in Appendix B.

While the nonlinearity introduced by X_i^C is useful as a mathematical illustration of the importance of chiral feedback, we now turn our attention to the agglomeration mechanism, and investigate whether it provides a sufficient chiral feedback in our model. Figure 3 illustrates the evolution of solid-phase enantiomeric excess for 100 simulations performed at otherwise identical conditions to Figure 2, but with agglomeration included. One can clearly see that all of the simulations evolve in a sigmoidal fashion to the expected final handedness. In some simulations, we observed that a small fraction of runs evolved sigmoidally to the wrong handedness due to a large fluctuation at early time which overcame the initial bias. Hence, the fidelity (i.e., the fraction of runs which evolve to the expected handedness) is not always 1. However, this behavior is a system size effect, and disappears with increasing system size. As with our artificial chiral feedback mechanism, agglomeration provides sufficient chiral feedback to drastically change the system behavior, reproducing the experimental evolution of ee^C. This result is also in agreement with the modeling efforts of Katsuno and Uwaha.[24]

The present model is capable of breaking symmetry when we begin with a perfectly racemic crystal population, with identical Gaussian crystal size distributions for both enantiomers. When simulations are performed with an initially racemic solid distribution, the final enantiomeric excess of the crystal population is either −1 or 1, with equal probability. For a given set of conditions, we also find that there can exist a significant variation in chiral induction time among runs. Some runs may quickly achieve an early-time symmetry breaking, and then proceed to enantiopurity, while other runs persist near the racemic state for significantly longer times until one enantiomer eventually gains sufficient excess to drive the crystal population to a homochiral state. This is illustrated in Figure 4, where our simulations are compared to experimental results of Hein *et al.*[5] For the simulations shown in Figure 4(a), all 100 runs eventually achieve crystalline enantiopurity in a sigmoidal fashion, and it seems reasonable to imagine that the runs in Figure 4(b) would eventually also achieve homochirality in longer experiments.

When considering whether agglomeration is an appropriate chiral feedback mechanism, it is desirable to look beyond the behavior of ee^C, and examine whether other experimental signatures are reproduced. We find that, as in experiments, the solution phase becomes transiently enriched in the enantiomer of opposite chirality to that which is prevalent in the crystal phase, as is shown in Figure 5. We also note that, for the agglomeration feedback mechanism, our model predicts transient ee^L values that are quite reasonable when

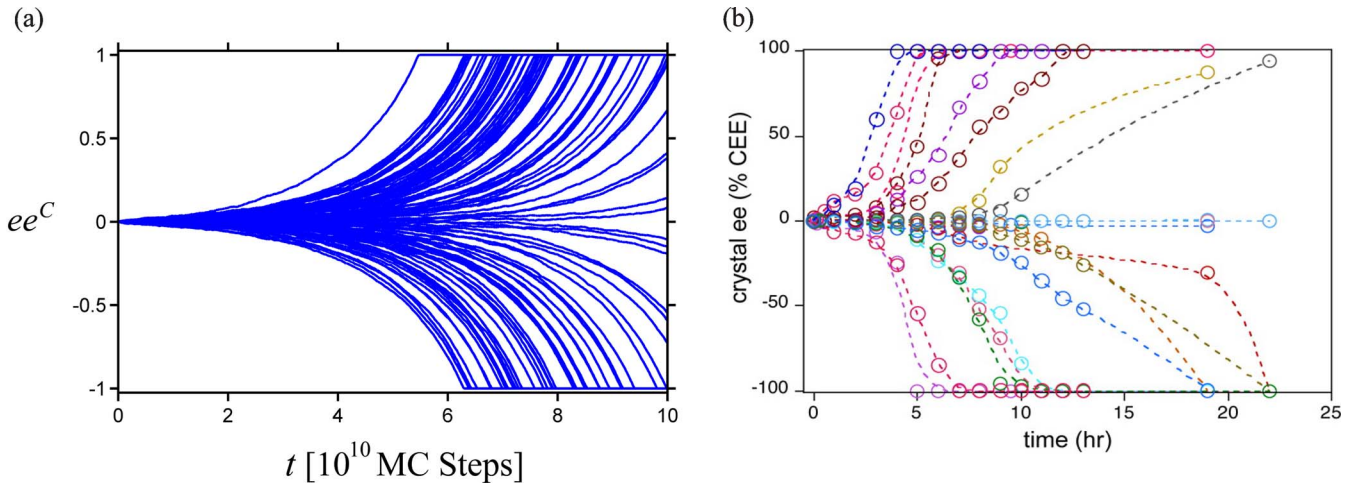

FIG. 4. Symmetry breaking with no initial bias, $ee^C(0) = 0$. (a) ee^C trajectories for 100 independent simulation runs. All runs performed with $\beta E_r = 5$, $p_{attr} = 0.4$, $K = 1$, $N_{total} = 206\,660$, $N^{eq} = 10\,000$. (b) ee^C trajectories for 24 independent Viedma ripening experiments, all performed under identical conditions. Chiral substance being deracemized is a conglomerate imine derivative of 2-Cl-phenylglycine, a component of the blockbuster drug, Plavix. Panel (b) reproduced by permission from Hein *et al.*, J. Am. Chem. Soc. **134**, 12629 (2012). Copyright 2012 American Chemical Society.

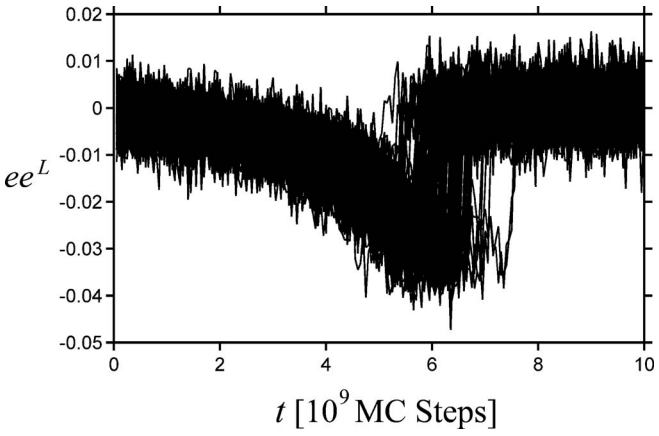

FIG. 5. Evolution of solution-phase enantiomeric excess. These trajectories are from the same 100 independent simulation runs used in Figure 3.

compared to those measured experimentally in the absence of racemization.[2] When the crystal phase has achieved enantiopurity, the solution rapidly racemizes and returns to chemical equilibrium, which is a racemic mixture of enantiomers.[2]

Our model assumes that any crystal above the minimum size for breakage, m_{min}, may undergo an attrition event. As a result, our initially Gaussian CSD rapidly becomes skewed towards smaller particle sizes. This is in qualitative agreement with recent experimental CSD measurements.[5] A typical CSD evolution for the model with agglomeration is shown in Figure 6, for which all simulation conditions are identical to those in Figure 5. Between 10^5 and 10^7 MC steps, the CSD becomes almost a simple exponential, and remains so throughout the duration of the simulation. Of course, the time until the quasi-steady CSD is reached, as well as the average width and size of the CSD, are all dependent on the probability of attrition, p_{attr}. In this case, by 10^{10} MC steps the system has gained crystal-phase enantiopurity in *R*, which is expected since in this case *R* was the enantiomer initially in excess in the solid.

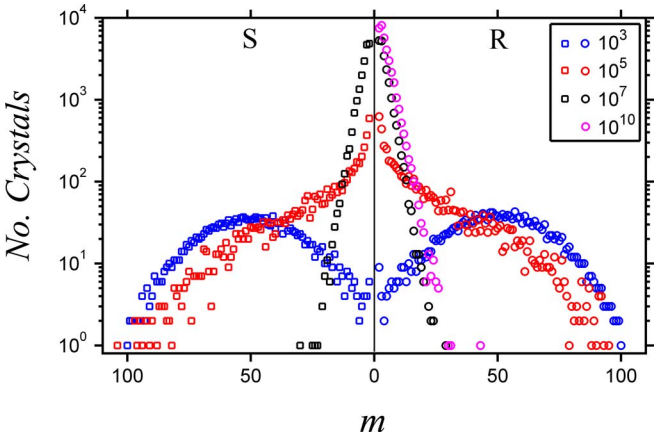

FIG. 6. Typical evolution of CSD for a single simulation run. Simulation began with initial bias, $ee^C(0) = 0.055$. On the left-hand side of the graph are the CSDs for the *S* enantiomer (squares), on the right-hand side are the CSDs for the R enantiomer (circles). The legend shows the correspondence between color and number of MC steps. Note that by 10^{10} MC steps, the crystal phase has achieved homochirality in *R*. All simulation parameters identical to Figures 3 and 5.

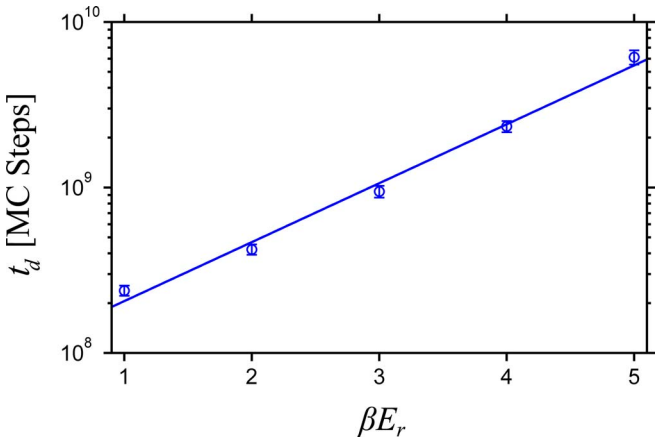

FIG. 7. Impact of solution-phase racemization rate on average crystal-phase deracemization time. Simulation began with initial bias $ee^C(0) = 0.055$. Averages are for 100 independent simulation runs. Error bars represent one standard deviation. The line is an exponential fit to the data: $t_d = 9.07 \times 10^7 * \exp(0.82 * \beta E_r)$, $R^2 = 0.9913$. All runs performed with $p_{attr} = 0.4$, $K = 1$, N_{total} 206 660, $N^{eq} = 10\,000$. The fidelity for all data points is 100/100.

We now address the influence of key model parameters on the deracemization time (i.e., the time it takes for the system to attain enantiopurity in the solid phase). Experimentally, the racemization rate during Viedma ripening is an important variable. Without the addition of a racemizing agent (i.e., 1,8-Diazabicycloundec-7-ene, commonly known as DBU[4,5]) racemization is usually very slow, and the Viedma ripening process becomes frustrated, preventing it from occurring on reasonable time scales. To explore the effect of racemization rate, we vary the activation energy barrier for racemization, βE_r, and observe how it changes the deracemization time. Referring to Figure 7, we see that the average deracemization time increases exponentially with the activation energy barrier. We model racemization as a first order process, hence the characteristic time for solution-phase racemization increases linearly with $\exp(\beta E_r)$. The results of Figure 7 indicate that the rate of racemization is a major bottleneck in the process, and thus determines the overall rate of Viedma ripening.

Another important parameter is the input of mechanical energy through vigorous stirring. In our model, that consideration is manifested as the probability of attrition, p_{attr}. The effects of varying p_{attr} are shown in Figure 8. In the limit of no attrition ($p_{attr} = 0$) no crystal breakage occurs, though the system remains well mixed. This scenario is analogous to performing Viedma ripening experiments in the absence of glass beads.[3] With no attrition, the Viedma ripening process is relatively slow due to the formation of large crystals via Ostwald ripening, and hence the average deracemization time is large, as suggested experimentally.[3] In this limit, homochirality is achieved when one, large crystal remains. As p_{attr} is increased from 0, the deracemization time rapidly decreases by an order of magnitude, due to the increased rate of mechanical breakage, and subsequent increase in the crystal population's total surface area. As p_{attr} is increased further, the average deracemization time becomes approximately constant in the range $0.4 \leq p_{attr} \leq 1$, with a shallow minimum occurring at $p_{attr} = 0.6$. In this range, increasing the rate of attrition does

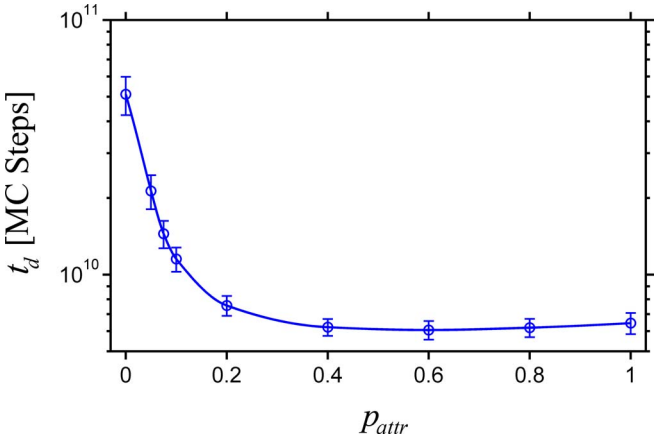

FIG. 8. Impact of attrition rate on average deracemization time. Simulation began with initial bias $ee^C(0) = 0.055$. Averages are for 100 independent simulation runs. Error bars represent one standard deviation, and the line is a guide to the eye. All runs performed with $\beta E_r = 5$, $K = 1$, $N_{total} = 206\,660$, $N^{eq} = 10\,000$. The fidelity for these data points is 100/100, with the exception of $p_{attr} = 0$ and $p_{attr} = 0.1$, for which the fidelity is 97/100 and 99/100, respectively. Runs which did not evolve to the expected handedness were discarded from calculation of average t_d.

little more than decrease the average crystal size, and shows no profound effect on t_d. The observation of a slight non-monotonicity in t_d vs. p_{attr}, coupled with similar results found in other simulation studies of this process,[23] led us to pursue the role of attrition further. We found that this non-monotonic behavior can be extended by increasing the intensity of an attrition event (i.e., by allowing some attrition events to break a crystal into more than two pieces). For more information on the effects of higher-intensity attrition, see the supplementary material.[31]

The final model parameter that can be varied is the ratio of rate constants for the growth and dissolution processes, $K = \delta/\alpha$. Referring to Figure 9, we find that at high values of K, when the dissolution rate is high, symmetry breaking occurs very rapidly. However, the high rates of dissolution result in very high supersaturations, which are not representative of the near-equilibrium process we are trying to model. At low values of K, growth begins to dominate over dissolution and there is not enough mass transfer between the two competing solids. In this limit, fluctuations in ee^C become more pronounced, and the system behavior tends to become more stochastic. The dependence of t_d on the rate at which molecules are able to dissolve has been suggested previously,[5] based on experimental results. In this work, we have used $K = 1$ for most calculations, as it maintains near-equilibrium supersaturation values but gives rise to sufficiently fast kinetics and adequate fidelity to achieve results consistent with experiment.

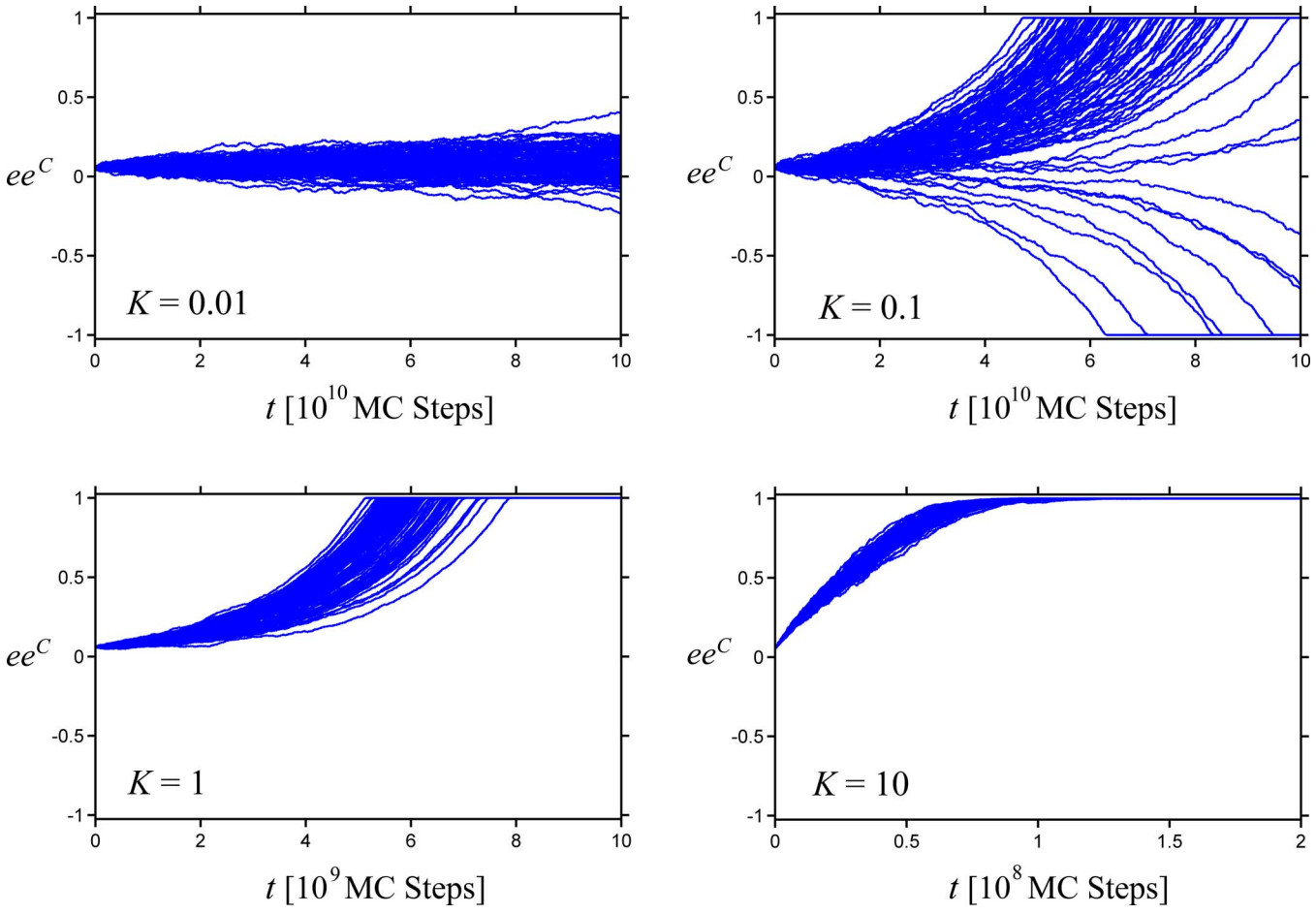

FIG. 9. Effect of K parameter. Simulation began with initial bias $ee^C(0) = 0.055$. Trajectories of 100 independent simulation runs are shown. Note the differences in time scale. All runs performed with $p_{attr} = 0.4$, $\beta E_r = 5$, $N_{total} = 206\,660$, $N^{eq} = 10\,000$.

IV. CONCLUSIONS

We have formulated and explored numerically a simple model, based on a small number of physical mechanisms, in order to study the key processes underlying Viedma ripening. The simplest formulation of the model, which we refer to as the elementary model, includes size dependent growth and dissolution, mechanical attrition, and solution-phase racemization, yet does not reproduce qualitatively the key experimental signatures. In this model, the crystal enantiomeric excess fluctuates in an unpredictable manner until the crystal population eventually achieves homochirality.

It is clear that the model requires a chiral feedback mechanism in order to reproduce key experimental signatures, as has been suggested elsewhere.[10,23,27] We have introduced two such feedback mechanisms: one purely mathematical, and the other based on a physical phenomenon, agglomeration, whose relevance to the Viedma ripening phenomenology remains a matter of discussion.[15] Both of these feedback mechanisms qualitatively reproduce experimental observations.

It is possible to rationalize why the agglomeration of small crystals onto other crystals could serve as a suitable chiral feedback mechanism. Agglomeration tends to increase the average size within a crystal population, while decreasing its net surface area. In addition, agglomeration of this type rescues small crystals from rapid dissolution and racemization. These self-reinforcing effects constitute a nonlinear crystal-phase phenomenon which in our model, as with others, is sufficient to reproduce the experimental behavior.

While our model builds on some of the insightful simulation work that has proceeded it,[23,24] we have chosen to make less restrictive assumptions and perform a more thorough exploration of the parameter space. Our systematic study of the parameter space illustrates the rich phenomenology that one can extract from such a simple model, and will hopefully enrich future mechanistic studies of this process. Racemization in the solution phase is a kinetic bottleneck of the Viedma ripening process with explicitly chiral molecules. Our results indicate that the solid-phase deracemization time increases linearly with the solution-phase racemization rate. The rate of attrition has a profound effect on the deracemization time, with low rates of attrition yielding slow Viedma ripening, and higher rates of attrition markedly speeding the deracemization process due to an increase in the total crystal surface area. In reproducing the crystal-phase evolution of enantiomeric excess, care must be taken with the choice of the relative rates of dissolution and growth rates, $K = \delta/\alpha$, which must be low enough to yield reasonably small supersaturations, yet high enough to enable sufficient mass transfer between the competing crystal populations.

One possible area for future inquiry is to study the separate influences of crystal size and crystal number that one uses to impose an initial enantiomeric bias. We have chosen to introduce initial enantiomeric bias by maintaining approximately the same mean crystal size for both populations (see Figure 1) since this is the simplest method of doing so. However, one could also use our model to study how a large number of small crystals comprising the minor enantiomer fares against a small number of large crystals of the major enantiomer.

Perhaps other subtle feedback mechanisms of physical significance have hitherto been overlooked, and will eventually be suggested. However, across a wide variety of models, it appears evident that a chiral feedback mechanism beyond size-dependent solubility is required in order to reproduce experimental observations. More detailed experimental studies focusing specifically on this aspect, particularly as it applies to the feasibility of the agglomeration process, are required.

ACKNOWLEDGMENTS

P.G.D. gratefully acknowledges the support of the National Science Foundation (NSF) (Grant No. CHE-1213343).

APPENDIX A: DERIVATION OF PHENOMENOLOGICAL CRYSTAL GROWTH RATE EQUATION

Consider the case of a macroscopic enantiopure crystal composed of chiral molecular species $i = \{R,S\}$ in contact with a liquid solution. At equilibrium, the liquid (volume V) will contain a saturated molecule number of species i, N^{eq}. Note N^{eq} is the same for both species R and S due to the Meyerhoffer double solubility rule.[30] We define the supersaturation of enantiomer i in the liquid as

$$\sigma_i(\infty) = \left(N_i^L - N^{eq}\right)/N^{eq}. \tag{A1}$$

This equation is identical to Eq. (3) in the main text. The inclusion of "∞" in the notation stresses the fact that this refers to the solubility of an infinitely large crystal.

For moderately small supersaturation ratios, whether positive or negative, the difference in chemical potentials between an arbitrarily large crystal of enantiomer i and a solution at fixed supersaturation, $\sigma_i(\infty)$, would be asymptotically proportional to $\sigma_i(\infty)$

$$\beta\left(\mu^C(\infty) - \mu_i^L\right) \sim -A\sigma_i(\infty), \tag{A2}$$

where $\beta = 1/k_BT$, k_B = Boltzmann's constant, T = absolute temperature, $\sigma_i(\infty)$ is the supersaturation of the liquid, $\mu^C(\infty)$ is the chemical potential of enantiomer i in an infinitely large enantiopure crystal, μ_i^L is the chemical potential of enantiomer i in the liquid solution, and A is a constant > 0. While Eq. (A2) is written for an infinitely large crystal in equilibrium with a solution, finite-size crystals have an additional contribution to the chemical potential due to liquid-crystal interfacial energetics. Hence, for an enantiopure crystal composed of m molecules of species i, the chemical potential increment over its dissolved form would have the following expected form:

$$\beta\left(\mu^C(m) - \mu_i^L\right) \sim -A\sigma_i(\infty) + Bm^{-1/3}, \tag{A3}$$

where dimensionless constant $B > 0$. The second term on the right-hand side of Eq. (A3) is proportional to the crystal's surface-to-volume ratio, assuming spherical crystals for simplicity. This last expression can formally be expressed in terms of a crystal-size-dependent effective supersaturation

ratio, σ_i (m), by setting

$$-A\sigma_i(m) = -A\sigma_i(\infty) + Bm^{-1/3}. \quad \text{(A4)}$$

Rearranging Eq. (A4), we have

$$\sigma_i(m) = \sigma_i(\infty) - (B/A)m^{-1/3}. \quad \text{(A5)}$$

When σ_i (∞) > 0, the thermodynamic driving force in this system is for large crystals to grow by acquiring molecules from the supersaturated solution. Note that the chemical potential increment expression, Eq. (A4), is positive for small crystals in the range

$$2 \le m < \left[\frac{B}{A\sigma_i(\infty)}\right]^3 \equiv m_i^*. \quad \text{(A6)}$$

Therefore, the thermodynamic driving force acting on these small crystals is to shrink in size, whereas the driving force for crystals of size $> m_i$* is to grow. These observations lead to a kinetic equation describing the average rate of change of crystal size m in terms of the effective supersaturation ratio

$$\langle d/dt\rangle\, m = \alpha\sigma_i(m)m^{2/3}, \quad \text{(A7)}$$

where $\langle d/dt\rangle m$ denotes the average rate of growth/dissolution of a crystal of size m, and $\alpha > 0$ is a fixed rate parameter. Note that the average rate of growth/dissolution in Eq. (A7) is proportional to the crystal's surface area. Substituting Eq. (A5), we obtain

$$\langle d/dt\rangle\, m = \alpha\sigma_i(\infty)m^{2/3} - (\alpha B/A)m^{1/3}. \quad \text{(A8)}$$

If we define $j = \langle d/dt\rangle m$, $\sigma_i = \sigma_i(\infty)$, and $\delta = \alpha B/A$, Eq. (2) is recovered identically.

APPENDIX B: ARTIFICIAL CHIRAL FEEDBACK

As mentioned in the main text, in order to reproduce the autocatalytic behaviors seen experimentally, it appears necessary to introduce a chiral feedback mechanism. This could be accomplished by considering additional growth mechanisms, such as agglomeration, or simply by artificially modifying the phenomenological crystal growth rate expression, as shown in Eq. (11), reproduced below as Eq. (B1),

$$j = \alpha\sigma_i X_i^C m^{2/3} - \delta m^{1/3}, \quad \text{(B1)}$$

where X_i^C = fraction of crystals which are of handedness i. By inserting X_i^C into the growth rate, whichever enantiomer comprises the major fraction of crystals ($X_i^C > 0.5$) gains an advantage in the growth rate over crystals of the opposite handedness. Solving for the critical size, $m_i^* = (K/(\sigma_i X_i^C))^3$.

As mentioned in the text, this nonlinearity is completely artificial, as the growth rate of a single crystal should not be directly influenced by the overall composition of the crystal population. However, as shown in Figure 10, when we insert this artificial nonlinearity into the elementary model, the model's behavior becomes markedly different. Despite the fact that all parameters are identical to the simulations in Figure 2, for all 100 simulations in Figure 10, ee^C now evolves in a sigmoidal fashion to homochirality in the handedness initially in excess. We also demonstrate that ee^L is temporarily enriched in the opposite enantiomer until homochirality is achieved in the solid and racemization returns the system to equilibrium, as measured experimentally.[2] Though we note that the extent of enantioenrichment in the solution for this set of conditions is significantly greater than that reported experimentally, the qualitative behavior is correct.

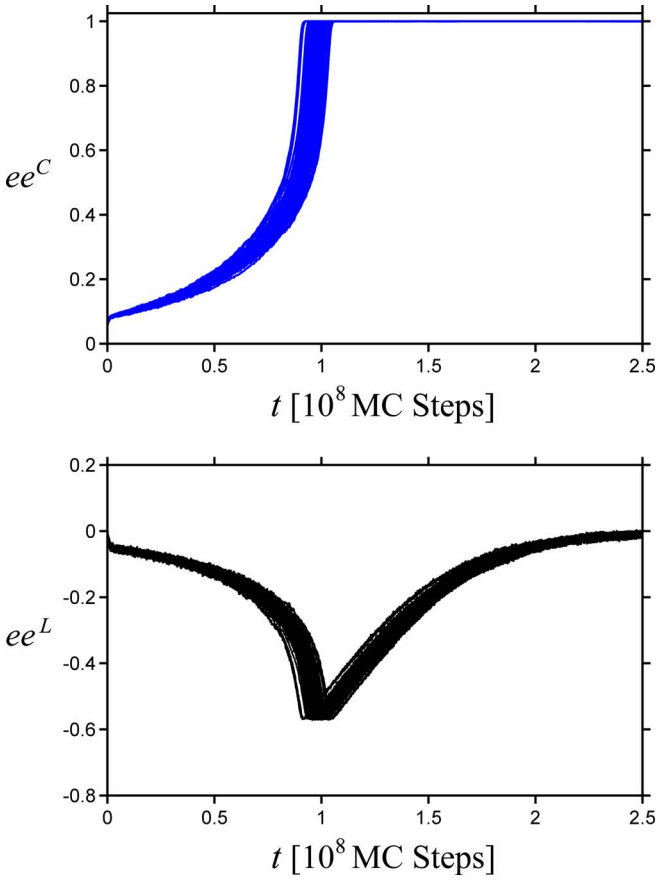

FIG. 10. Evolution of crystal-phase and liquid-phase enantiomeric excess for the elementary model with artificial chiral feedback mechanism, Eq. (11). Simulations began with initial bias, $ee^C(0) = 0.055$. Trajectories of 100 independent simulation runs are shown. (Top) Crystal enantiomeric excess. (Bottom) Solution enantiomeric excess. All simulation parameters identical to Figure 2.

In order to test the strength of this nonlinear term, we studied how decreasing the contribution of X_i^C affects the time to enantiopurity (deracemization) in the crystal, t_d, and

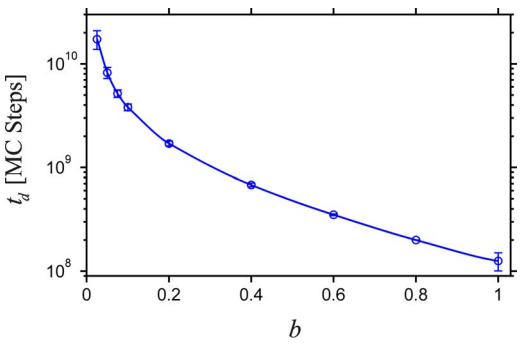

FIG. 11. Dependence of the average deracemization time upon phenomenological kinetic exponent, b. Simulations began with initial bias $ee^C(0) = 0.055$. Averages are for 100 independent simulation runs. Error bars represent one standard deviation. All simulation parameters identical to Figure 2. The fidelity for all points is 100/100.

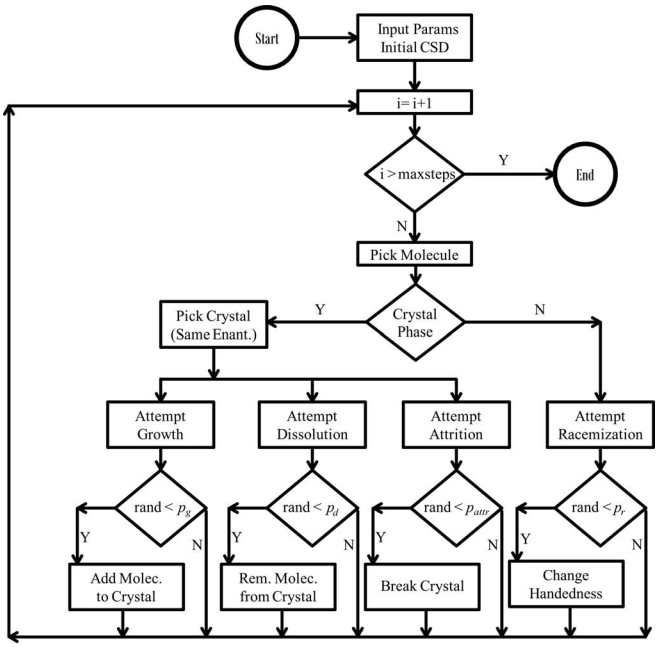

FIG. 12. Algorithm flowchart for elementary model.

the fidelity of the simulations to propagate the initially imposed enantiomeric excess. We modify Eq. (B1) with an adjustable parameter, b, as shown in Eq. (B2). This modification changes the definition of the critical crystal size to: $m_i^* = (K/(\sigma_i(X_i^C)^b))^3$

$$j = \alpha\sigma_i \left(X_i^C\right)^b m^{2/3} - \delta m^{1/3}. \tag{B2}$$

The effect of decreasing b from 1, where we have the full effect of the chiral feedback, to 0, where we identically recover the elementary model, is depicted in Figure 11. One can see that, as the parameter b is decreased, the deracemization time increases by orders of magnitude. For this system size, $N_{total} = 206\,660$, the fidelity (fraction of runs which evolve to the expected handedness in the crystal phase) remains 100% until b becomes less than 0.025. As b is decreased below 0.025, the erratic behavior typical of the elementary model (see Figure 2) becomes increasingly prevalent, with the deracemization time and its standard deviation rapidly increasing, and the fidelity rapidly decreasing.

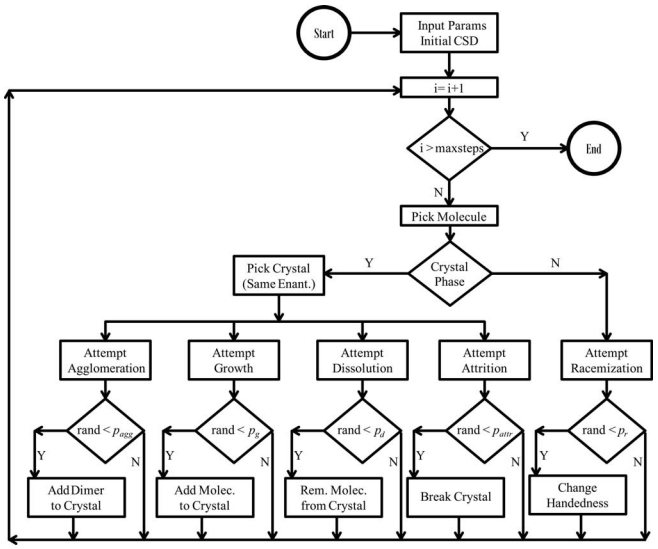

FIG. 13. Algorithm flowchart for model with agglomeration.

APPENDIX C: ALGORITHM FLOWCHARTS

See Figs. 12 and 13.

[1]C. Viedma, "Chiral symmetry breaking during crystallization: Complete chiral purity induced by nonlinear autocatalysis and recycling," Phys. Rev. Lett. **94**(6), 065504 (2005).
[2]W. L. Noorduin, W. J. P. van Enckevort, H. Meekes, B. Kaptein, R. M. Kellogg, J. C. Tully, J. M. McBride, and E. Vlieg, "The driving mechanism behind attrition-enhanced deracemization," Angew. Chem., Int. Ed. **49**(45), 8435–8438 (2010).
[3]C. Viedma, J. E. Ortiz, T. de Torres, T. Izumi, and D. G. Blackmond, "Evolution of solid phase homochirality for a proteinogenic amino acid," J. Am. Chem. Soc. **130**(46), 15274–15275 (2008).
[4]W. L. Noorduin, T. Izumi, A. Millemaggi, M. Leeman, H. Meekes, W. J. P. Van Enckevort, R. M. Kellogg, B. Kaptein, E. Vlieg, and D. G. Blackmond, "Emergence of a single solid chiral state from a nearly racemic amino acid derivative," J. Am. Chem. Soc. **130**(4), 1158–1159 (2008).
[5]J. E. Hein, B. H. Cao, C. Viedma, R. M. Kellogg, and D. G. Blackmond, "Pasteur's tweezers revisited: On the mechanism of attrition-enhanced deracemization and resolution of chiral conglomerate solids," J. Am. Chem. Soc. **134**, 12629–12636 (2012).
[6]D. G. Blackmond, "The origin of biological homochirality," Cold Spring Harbor Perspect. Biol. **2**(5), a002147 (2010).
[7]W. L. Noorduin, P. van der Asdonk, A. A. C. Bode, H. Meekes, W. J. P. van Enckevort, E. Vlieg, B. Kaptein, M. W. van der Meijden, R. M. Kellogg, and G. Deroover, "Scaling up attrition-enhanced deracemization by use of an industrial bead mill in a route to Clopidogrel (Plavix)," Org. Process Res. Dev. **14**(4), 908–911 (2010).
[8]J. W. Gibbs, *Thermodynamics, Collected Works* (Yale University Press, New Haven, CT, 1948), Vol. I.
[9]W. Ostwald, *Lehrbuch der Allgemeinen Chemie*, Part 1 (Leipzig, Germany, 1896), Vol. 2.
[10]M. Uwaha, "A model for complete chiral crystallization," J. Phys. Soc. Jpn. **73**(10), 2601–2603 (2004).
[11]J. M. McBride and J. C. Tully, "Physical chemistry: Did life grind to a start?," Nature (London) **452**(7184), 161–162 (2008).
[12]D. K. Kondepudi, R. J. Kaufman, and N. Singh, "Chiral symmetry-breaking in sodium-chlorate crystallization," Science **250**(4983), 975–976 (1990).
[13]D. K. Kondepudi, K. L. Bullock, J. A. Digits, J. K. Hall, and J. M. Miller, "Kinetics of chiral-symmetry breaking in crystallization," J. Am. Chem. Soc. **115**(22), 10211–10216 (1993).
[14]T. Buhse, D. Durand, D. Kondepudi, J. Laudadio, and S. Spilker, "Chiral symmetry breaking in crystallization: The role of convection," Phys. Rev. Lett. **84**(19), 4405–4408 (2000).
[15]C. Viedma, J. M. McBride, B. Kahr, and P. Cintas, "Enantiomer-specific oriented attachment: Formation of macroscopic homochiral crystal aggregates from a racemic system," Angew. Chem., Int. Ed. **52**, 10739–10742 (2013).
[16]S. B. Tsogoeva, S. Wei, M. Freund, and M. Mauksch, "Generation of highly enantioenriched crystalline products in reversible asymmetric reactions with racemic or achiral catalysts," Angew. Chem., Int. Ed. **48**(3), 590–594 (2009).
[17]S. W. Wei, M. Mauksch, and S. B. Tsogoeva, "Autocatalytic enantiomerisation at the crystal surface in deracemisation of scalemic conglomerates," Chem.-Eur. J. **15**(39), 10255–10262 (2009).
[18]C. Viedma, B. J. V. Verkuijl, J. E. Ortiz, T. de Torres, R. M. Kellogg, and D. G. Blackmond, "Solution- phase racemization in the presence of an enantiopure solid phase," Chem.-Eur. J. **16**(16), 4932–4937 (2010).
[19]M. Uwaha, "Simple models for chirality conversion of crystals and molecules by grinding," J. Phys. Soc. Jpn. **77**(8), 083802 (2008).
[20]M. Uwaha and H. Katsuno, "Mechanism of chirality conversion by grinding crystals: Ostwald Ripening vs crystallization of chiral clusters," J. Phys. Soc. Jpn. **78**(2), 023601 (2009).

[21]M. Uwaha and K. Koyama, "Transition from nucleation to ripening in the classical nucleation model," J. Cryst. Growth **312**(7), 1046–1054 (2010).
[22]M. Uwaha, "Steady chirality conversion by grinding crystals—Supercritical and subcritical bifurcations," J. Cryst. Growth **318**(1), 89–92 (2011).
[23]W. L. Noorduin, H. Meekes, A. A. C. Bode, W. J. P. van Enckevort, B. Kaptein, R. M. Kellogg, and E. Vlieg, "Explanation for the emergence of a single chiral solid state during attrition-enhanced Ostwald ripening: Survival of the fittest," Cryst. Growth Des. **8**(5), 1675–1681 (2008).
[24]H. Katsuno and M. Uwaha, "Monte Carlo simulation of a cluster model for the chirality conversion of crystals with grinding," J. Cryst. Growth **311**(17), 4265–4269 (2009).
[25]Y. Saito and H. Hyuga, "Chiral crystal growth under grinding," J. Phys. Soc. Jpn. **77**(11), 113001 (2008).
[26]Y. Saito and H. Hyuga, "Grinding-induced homochirality in crystal growth," J. Cryst. Growth **318**(1), 93–98 (2011).
[27]M. Iggland and M. Mazzotti, "A population balance model for chiral resolution via Viedma ripening," Cryst. Growth Des. **11**(10), 4611–4622 (2011).
[28]P. J. Skrdla, "Kinetics and thermodynamics of efficient chiral symmetry breaking in nearly racemic mixtures of conglomerate crystals," Cryst. Growth Des. **11**(5), 1957–1965 (2011).
[29]J. H. E. Cartwright, O. Piro, and I. Tuval, "Ostwald ripening, chiral crystallization, and the common-ancestor effect," Phys. Rev. Lett. **98**(16), 165501 (2007).
[30]W. Meyerhoffer, "Stereochemical notices," Ber. Dtsch. Chem. Ges. **37**, 2604–2610 (1904).
[31]See supplementary material at http://dx.doi.org/10.1063/1.4827478 for additional notation definitions, high-intensity attrition behavior, and an alternative phenomenological rate expression.
[32]R. David, P. Marchal, J. P. Klein, and J. Villermaux, "Crystallization and precipitation engineering-III. A discrete formulation of the agglomeration rate of crystals in a crystallization process," Chem. Eng. Sci. **46**(1), 205–213 (1991).
[33]C. Lindenberg, J. Scholl, L. Vicum, M. Mazzotti, and J. Brozio, "L-glutamic acid precipitation: Agglomeration effects," Cryst. Growth Des. **8**(1), 224–237 (2008).
[34]H. Katsuno and M. Uwaha, "Appearance of a homochiral state of crystals induced by random fluctuation in grinding," Phys. Rev. E **86**(5), 051608 (2012).